ACS APPLIED MATERIALS & INTERFACES

Research Article

www.acsami.org

Influence of Texture Coefficient on Surface Morphology and Sensing Properties of W-Doped Nanocrystalline Tin Oxide Thin Films

Manjeet Kumar,[†] Akshay Kumar,[‡] and A. C. Abhyankar*,[†]

[†]Department of Materials Engineering, Defence Institute of Advanced Technology (DU), Girinagar, Pune 411025, India

[‡]Department of Nanotechnology, Sri Guru Granth Sahib World University, Fatehgarh Sahib, Punjab-140406, India

Supporting Information

ABSTRACT: For the first time, a new facile approach based on simple and inexpensive chemical spray pyrolysis (CSP) technique is used to deposit Tungsten (W) doped nanocrystalline SnO_2 thin films. The textural, optical, structural and sensing properties are investigated by GAXRD, UV spectroscopy, FESEM, AFM, and home-built sensing setup. The gas sensing results indicate that, as compared to pure SnO_2, 1 wt % W-doping improves sensitivity along with better response (<2 s) and recovery time (<25 s) toward NO_2 gas at operating temperatures of ~225 °C. The optimal composition of 1 wt % W-doped films exhibit lowest crystallite size of the order of ~8−10 nm with reduced energy band gap and large roughness values of 3.82 eV and 3.01 nm, respectively. Reduction in texture coefficient along highly dense (110) planes with concomitant increase along loosely packed (200) planes is found to have prominent effect on gas sensing properties of W-doped films.

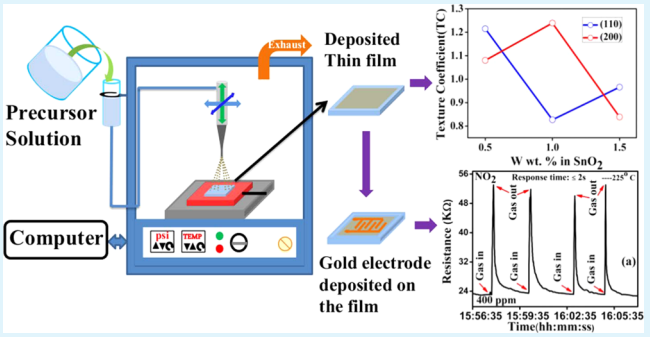

KEYWORDS: *tin oxide, thin films, texture coefficient, chemical spray pyrolysis, gas sensors*

1. INTRODUCTION

In the past decade, researchers have made rapid and significant advances in the field of chemical gas sensors. Among the solid state gas sensors, metal oxide based resistive sensors are most widely studied and used for various applications ranging from domestic front to space program.[1] SnO_2 a wide band gap (3.6 eV) n-type semiconductor and its variety of nanostructured forms[2−8] are used extensively for gas sensing applications because of their good chemical stability and highly reproducible ppm to ppb level sensitivity.[9] Moreover, selectivity in pure SnO_2, for large number of pollutants and chemically hazardous gases can be tuned/improved by doping of transition metals and rare earths elements.[10] Recent experimental[11] and computational studies[12] are focused on crystallinity, morphology and specific surfaces (Miller planes) as sensitivity is known to have strong influence on different facets of crystals because geometrical, electronic and chemical properties are highly anisotropic. Hence, functionality of sensor materials depends not only on spatial dimensions and composition but also on crystal surfaces that are exposed to gas analytes. Thus, to reveal the mechanisms of gas sensing in nanosensors,[13] three important steps are emphasized, namely, (a) to perform gas sensing measurements, (b) computation modeling, and (c) in situ spectroscopic studies (under operating conditions), on specific surfaces. However, all these measurements require sophisticated equipments and high-end characterization techniques, as well and in real conditions large deviations from in situ measurements are expected. Because, to gain fundamental understanding of gas adsorption stringent requirements such as creation of only one type of surface (set of equivalent Miller planes), same morphology at different length scales over large surface area with better sensitivity are to be fulfilled. SnO_2 thin films deposited by simple chemical spray pyrolysis (CSP) technique are known to exhibit variety of crystalline shapes and sizes, which are strongly depend on deposition temperatures and film thicknesses. These facts are also verified by computer image simulations.[14] Thus, the effect of texture can be investigated in CSP assembled thin films. There are a few other advantages of CSP regarding doping of samples. Doping of different atomic elements is often possible whose salt can be dissolved in the spray solution with SnO_2 and most importantly, this method is suitable for large area deposition. For example, thin film sensors of as large as 15 cm × 15 cm areas can be deposited in laboratory scale spray pyrolysis set up (HOLMARC Spray Pyrolysis Equipment Model No. HO-TH-04).

The recent efforts to check environmental pollution and thereof increased awareness to monitor the potentially hazardous gases have stimulated considerable research and development in the field of gas sensors. NO_2 being widely produced by power plants, motor vehicles, residential, commercial, and industrial burning fuels is also hazardous in nature, and causes eye, nose and throat irritations.[15] The exposure of NO_2 triggers a variety of health problem including

Received: October 26, 2014
Accepted: January 20, 2015
Published: January 20, 2015

DOI: 10.1021/am507397z
ACS Appl. Mater. Interfaces 2015, 7, 3571−3580

Table 1. Synthesis Techniques and Gas Sensing Response, Recovery, and Response Time Values of Sensors Used for NO_2 Detection from Literature

materials used	catalyst used	deposition technique	sensor response	response time (s)	recovery time (s)	ref
SnO_2 thin film	none	RF sputtering	2.9× 10^4 (50 ppm)	96	>1800	19
SnO_2 thin film	WO_3 disc	RF sputtering	5.4× 10^4 (10 ppm)	67	1025	20
SnO_2 thin film	MoO_3	sol−gel spin coating	3.6 (500 ppm)	2	180−240	23
SnO_2 thin film	WO_3	sol−gel spin coating	33359 (500 ppm)	<2	90	24
WO_3 nanotubes	none	thermal evaporation method	677 (50 ppm)	30	75	25
WO_3 nanorods			326 (50 ppm)	75	100	
WO_3	none	sol−gel dip coating	3.37 (2 ppm)	120	>1200	26

diaphoresis (sweating), worsening cough, choking, asthma, reduced lung capacity, and increase the risk of respiratory symptoms.[16,17] Because of these detrimental effects of NO_2 emission on health and environment; reproducible, selective, and parts per million/parts per billion level detection is an innovative and intensive research topic. Surface sensitization of porous SnO_2 films was reported[18] by using nanoclusters like ZnO and WO_3; in that sensitivity for NO_2 is remarkably improved by incorporation of WO_3 nanoclusters.[19,20] Although, WO_3−SnO_2 heterostructures are studied extensively for NO_2 detection, relatively less literature is available for W-doped SnO_2.[21] Although many recent reports are published on the crystal plane dependent structural modifications and its effect on transport properties,[10,22] the majority of work is carried on thin films synthesized either by sputter coating or PLD. In that, a very few reports are available that correlates textural, optical, microstructural and gas sensing properties of metal oxides including SnO_2. To the best of our knowledge, no report is available on chemical spray pyrolysis (CSP) based synthesis of W-doped SnO_2 nanostructured films. Table 1 displays sensitivity, operating temperatures, response, and recovery times of some NO_2 sensors, wherein, WO_3−SnO_2 composite sensor is found to have superior sensitivity as compared to SnO_2 and other sensors.[19,20,22−26] Although, response times of WO_3−SnO_2 are good and recovery time of these sensors are in the range of 75−1800 s.

In this context, we report textural properties, estimated by grazing angle XRD measurements, of W-doped SnO_2 thin films deposited by a simple and inexpensive CSP method. Surface morphology, microstructure, and band gap energy (E_g) of the films are examined by atomic force microscopy (AFM), field emission electron microscopy (FESEM) and UV spectroscopy, respectively. The calculated texture coefficient, roughness of the films, crystallite size and band gap energies are correlated to NO_2 sensitivity. The W-doped sensors exhibits good response time and extremely fast recovery time as compared to literature as shown in Table 1. The present work reveals that changes in atomic density of (110) and (200) Miller planes of W-doped SnO_2 thin film sensor have strong influence on sensitivity and selectivity for NO_2 which is also reflected in surface morphology, roughness, band gap and crystallite size. Thus, one can study the effect of texture coefficient on gas adsorption properties in CSP assembled thin films, although it is small but important step in understanding the fundamentals of gas adsorption on specific crystal facets as mentioned in the recent literature.[13,27]

2. EXPERIMENTAL SECTION

2.1. Synthesis. Thin films of pure and W-doped SnO_2 with various concentrations were deposited using CSP technique on glass substrates. In this experiment $SnCl_4.5H_2O$ was dissolved in an appropriate amount of propanol. The WCl_6 with different mass ratio of W/Sn was added to the solution. Thereafter thorough mixing was done using an ultrasonicator bath for 45 min. Amorphous glass microslides substrates were cleaned thoroughly.[28] These films were deposited on substrate at the temperature of 450 °C. The substrates were kept on a heater and temperature was measured at the surface of substrate by using thermocouple. To deposit the film with the reproducible properties, a very small variation in the deposition temperature (±3 °C) was maintained at the substrate. The chemical solution to be sprayed was introduced by a dispenser through a tube at the liquid inlet of the atomizer. Compressed air was let into the gas inlet after passing through dust filter. A separate gas regulator was used to maintain pressure of the gas. The solution flow rate and gas flow rate were maintained at 3 mL/min and 50 psi, respectively. The distance between the substrate and nozzle was maintained constant (20 cm) throughout deposition time (2 min). The drop in the substrate temperature during the deposition was found to be ∼30 °C, for all the deposited films. The sintering of these deposited films was carried out at temperature of 500 °C for 6h using a muffle furnace and was cooled down at the rate of 100 °C per hour.

2.2. Characterization. The crystallographic study was carried out using Bruker AXS, Germany (Model D8 Advanced) diffractometer in the scanning range of 20−80° (2θ) using Cu−K_α radiations with wavelength 1.54 Å. Roughness and topography of these films were studied by using atomic force microscopy (AFM, Asylum Research), operating in tapping mode. Surface morphology and chemical composition of sensor films were determined using (FESEM) Model Σigma, Carl Ziess. Dual beam UV−vis spectrophotometer (PerkinElmer Lambda 900) having an integrating sphere was employed for measuring the optical properties. Gas sensing experiments were performed with an indigenously built gas sensing setup attached with mass flow controllers for precise measurement of gas flow at parts per million level.[28] Gold pattern electrodes were evaporated on the sensing layer and the film area, 0.51 cm^2, was kept constant for all the sensor films during gas sensing measurements. The operating temperature was varied from 100 to 350 °C in order to find out the optimum working temperature of these deposited films for NO_2 gas sensing. Change in resistance of the sensor films was measured as a function of time through a computer interfaced EXTECH MultiMaster 560A True RMS digital multimeter.

3. RESULTS

The structural studies have been carried out by using GAXRD (grazing angle X-ray diffraction) measurements in the range of 2θ from 20 to 80 degrees. GAXRD patterns of deposited SnO_2 thin films are shown in Figure 1a. The obtained diffraction patterns of pure and W-doped SnO_2 were compared with JCPDS data card no. 088-0287, which confirmed that the thin films have tetragonal rutile phase with space group $P42/mnm$. Rietveld refinement of the diffraction patterns is performed to check phase purity, to determine the lattice constants and average crystallite size of the thin films and these values are tabulated in Table 2. The lattice parameter a of the unit cell is found to increase linearly with the W-concentration up to 1 wt % following Vegards law and reduces thereafter for 1.5 wt %

DOI: 10.1021/am507397z
ACS Appl. Mater. Interfaces 2015, 7, 3571−3580

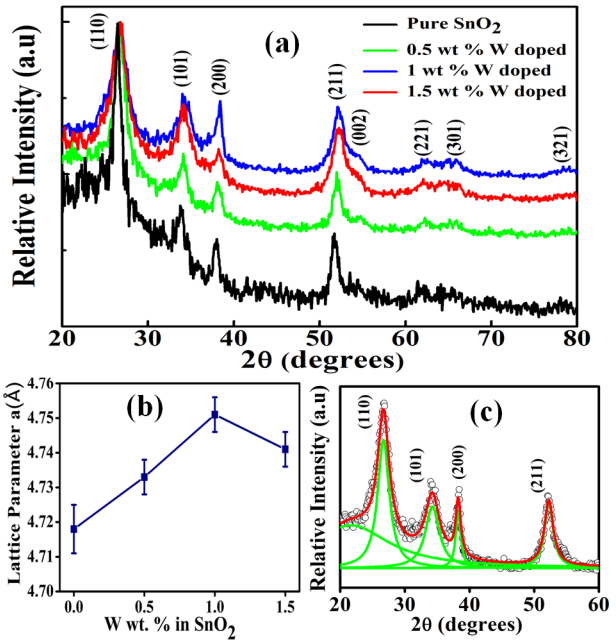

Figure 1. (a) XRD patterns of pure and W-doped SnO_2 deposited at 450 °C. (b) Lattice parameter *a* as a function of W doping and (c) shows procedure of calculation for integrated intensity corrected for amorphous background.

shown in Figure 1b. It is also observed that the full width at half maxima (fwhm) increases with an increase in W content in the SnO_2 thin films up to 1 wt % and reduces for 1.5 wt %. Accordingly lowest average crystallite size of 8 nm is estimated for 1 wt % W-doped films. This suggests that W substitution in the SnO_2 lattice results in a decrease in crystallite size up to 1 wt %. These observations suggest that W already substitutes in SnO_2 lattice.

The degree of preferred orientation of the different crystalline planes can be determined from the Harris's analysis,[29] by calculating the texture coefficient as per eq 1

$$P(h_i k_i l_i) = \frac{I(h_i k_i l_i)}{I_0(h_i k_i l_i)} \left[\frac{1}{n} \sum_{i=1}^{n} \frac{I(h_i k_i l_i)}{I_0(h_i k_i l_i)} \right]^{-1} \quad (1)$$

where $P(hkl)$ is the texture coefficient of the plane specified by Miller Indices (hkl); $I(hkl)$ and $I_0(hkl)$ are the integrated intensity ratios of the thin films and bulk randomly oriented SnO_2 powder respectively, for a given peak and n is the number of diffraction peaks. In order to calculate the correct integrated intensity ratios, the amorphous background emanating from glass substrate needs to be removed by following procedure: As the diffraction pattern of all the sensor films contain only four intense diffraction peaks from (110), (101), (200), and (211) miller planes; they were fitted with four Lorentzian peaks, additionally amorphous background was modeled as a fifth Lorentzian peak, as shown in Figure 1c. The amorphous background is thus deconvoluted from each Bragg peak and integrated intensity corresponding to each peak was calculated. These intensities were then compared with bulk samples as per formula given in eq 1 to calculate the texture coefficients of Miller planes in diffraction patterns of thin film. These results are tabulated in Table 3. An increase (decrease) from the unity

Table 3. Texture Coefficients Calculated from Integrated Intensity Ratios for Respective Miller Planes

	texture coefficient			
planes (*hkl*)	pure SnO_2	0.5 wt % W-doped	1 wt % W-doped	1.5 wt % W-doped
110	1.479	1.074	0.794	0.914
101	0.611	0.632	0.631	0.688
200	1.470	1.767	2.016	1.817
211	0.440	0.526	0.557	0.579

in the texture coefficient indicates a higher (lower) degree of preferred orientation along a particular plane of the film with respect to bulk SnO_2. The deviation in the texture coefficient from unity for a particular Miller plane also corresponds to change in atomic densities corresponding to that plane as X-ray intensities are function of atomic structure factors.[30] Thus, higher (lower) value of the texture coefficient actually corresponds to increase (decrease) in planar density along a particular crystal plane as compared to ideal values. The texture analysis thus indicates that pure SnO_2 is highly textured along (110) plane. However, with the substitution of tungsten in SnO_2, the texture coefficient of (200) plane increases remarkably with concomitant decrease in (110) which results in reduced planar density on (110) plane up to 1 wt % of W-doping. As shown in Figure 2a and b, the planar density is highest for (110) plane as compared to (200) plane. In these calculations, I_0 value is taken from ICDD file which normally measured in Bragg–Brentano geometry. Now that intensities of W-doped thin films may have inherent contribution to texture due to thin film measurement geometry, the absolute values of calculated texture coefficients may not be accurate. However, peak intensities of thin films are normalized with ASTM standard bulk randomly oriented SnO_2 powder as per Harris formula given in eq 1 and thus, comparison between the texture coefficients for W-doped thin films can yield information regarding the changes in atomic planar densities. In order to avoid errors in texture coefficients resulting from two different X-ray measurement geometries, texture coefficients are recalculated using I_0 values from pure SnO_2 thin film. The texture coefficients of (110) and (200) plane are then plotted as a function of W concentration as shown in Figure 2(c). It reveals a very important result that (110) planar density

Table 2. Average Crystallite Size, RMS Roughness, Texture Coefficient, Band Gap, Lattice Parameter, and Sensing Response for Pure and W-Doped SnO_2

					lattice parameter		
W wt. % in SnO_2	av crystallite size (nm)	RMS roughness (nm)	texture coefficient (***200***)	band gap (eV)	*a* (Å)	*c* (Å)	sensors response
0	18 ± 3	1.25	1.470	3.97 ± 0.02	4.718(7)	3.182(6)	26
0.5	15 ± 3	1.36	1.767	3.88 ± 0.03	4.733(5)	3.189(4)	37
1	6 ± 2	3.01	2.016	3.82 ± 0.03	4.751(5)	3.159(4)	132
1.5	13 ± 4	1.5	1.817	3.87 ± 0.01	4.741(5)	3.173(4)	54

DOI: 10.1021/am507397z
ACS Appl. Mater. Interfaces 2015, 7, 3571−3580

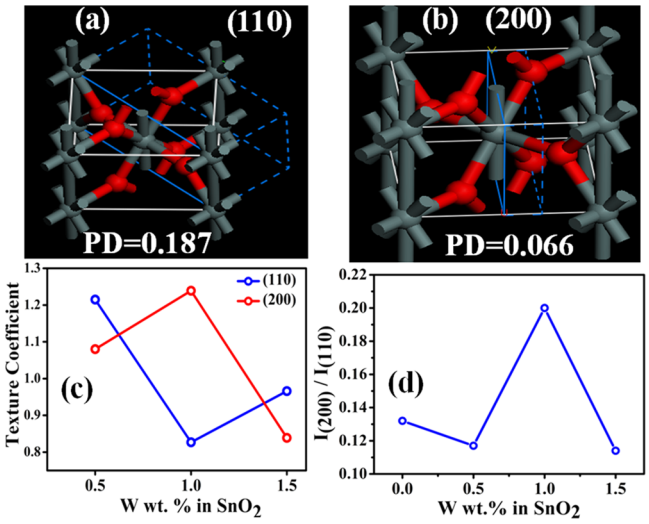

Figure 2. (a and b) Theoretically calculated planar density (PD) of (110) and (200) plane of SnO_2. (c) Texture coefficient as a function of W doping, and (d) intensity ratios (I_{200}/I_{110}) as a function of W doping.

decreases drastically with concomitant increase of (200) planar density in case of 1 wt % W-doped thin films as texture coefficients drops down to ∼0.8 in case of (110) plane and increase to ∼1.3 for (200) plane. No such changes are observed for 0.5 and 1.5 wt % W-doped thin films instead texture coefficients of (110) is slightly higher than (200) plane and both are near unity. The similar inferences can also be drawn in case of texture coefficients estimated using ASTM standard intensities for SnO_2 powder, where largest increase in TC of (200) plane is observed at the cost of (110) plane (see Table 3). The present analysis thus confirms that many vacancies lie on (110) plane in case of 1 wt % W-doped films. Effects of these changes on gas sensing properties have been discussed at the end of this section.

To estimate optical band gap and transparency, ultraviolet−visible (UV−vis) spectrophotometry measurements were performed in the range of 200 to1200 nm for pure and W-doped SnO_2 thin films. Direct band gap values were determined from the Tauc plots as shown in Figure 3 for pure and W-doped SnO_2 thin films. Inset a of Figure 3 shows the variation of transmittance with photon wavelength where thickness of thin films was maintained ∼120 nm. It is observed that the transmittance of the pure SnO_2 film is lowest, 86%, in the visible region which increases up to 96% to 98% upon W-doping in the visible region. All the thin films exhibit very high visible transparency around 86−98%, which also confirms the crystalline nature of the thin films.[21] From the Tauc plot, it is evident that the band gap decreases with W-doping up to 1 wt % in SnO_2. However, the decrease in band gap is very small. The lowest band gap of 3.82 eV is estimated for 1 wt % W-doped thin film.

FESEM micrographs of pure and W-SnO_2 thin films are shown in Figure 4a−d, which reveals that the films are uniform with densely packed nanosized polygonal equi-axed grains. The average grain size values estimated using ImageJ software for these micrographs. The analysis reveals that 1 wt % W-doped films has the lowest average grain size of ∼10 nm whereas grain sizes of ∼30 nm is observed for pure SnO_2, 0.5 and 1.5 wt % W-doped films. Figure 4e reveals a cross-sectional view of the W-SnO_2 films. The thickness of the films was found to be ∼120 nm. Figure 5a−d shows the EDS spectrum of pure and W-doped SnO_2 which reveals presence of Sn, O, and W in requisite compositions. No other impurity phases were detected. It also rules out the presence of monoclinic WO_3 phase, consistent with single phase XRD peaks as shown in Figure 1. With W-doping up to 1 wt % large decrease in crystallite size ∼10 nm is observed. Another important feature of the 1 wt % microstructure is clustering of nanosized grains with porous network as compared to other films which is further investigated by atomic force microscope (AFM) studies. The variation of crystallite size with composition observed in

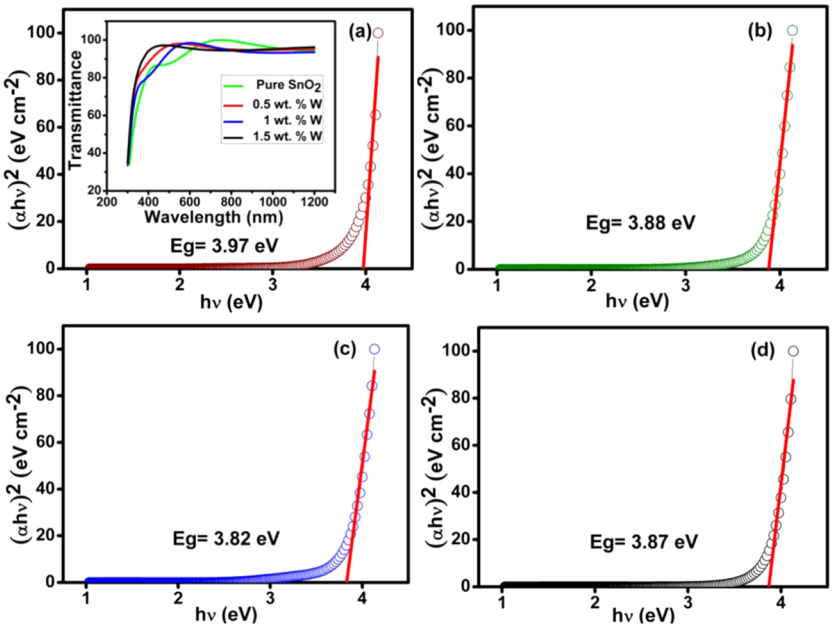

Figure 3. Tauc plots of (a) pure SnO_2, (b) 0.5 wt % W-doped SnO_2, (c) 1 wt % W-doped SnO_2, and (d) 1.5 wt % W-doped SnO_2 for the estimation of band gap energy. Inset in panel a shows the variation of optical transmittance of pure and W-doped SnO_2 thin films with wavelength.

DOI: 10.1021/am507397z
ACS Appl. Mater. Interfaces 2015, 7, 3571−3580

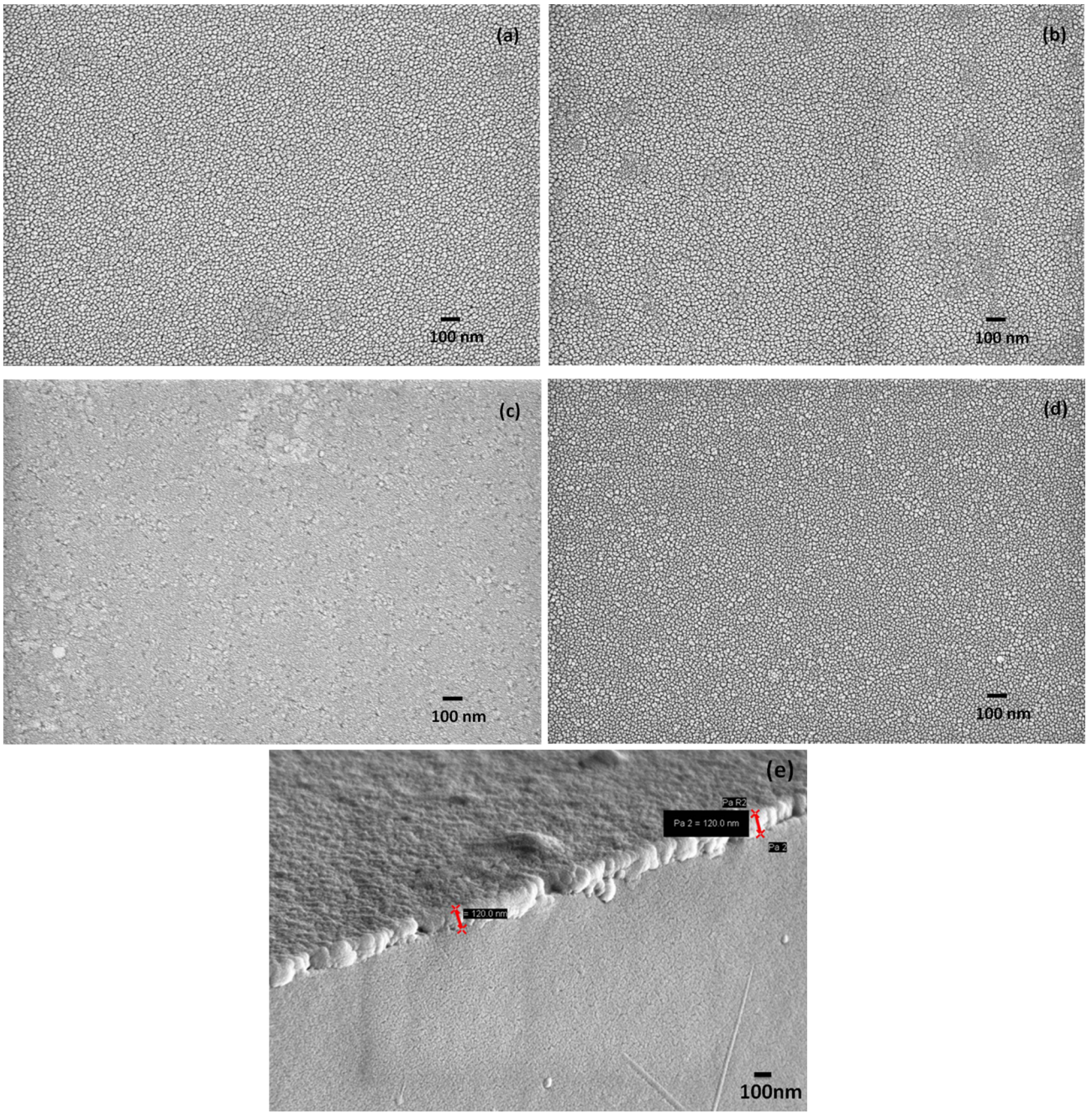

Figure 4. FESEM micrographs of (a) pure SnO_2, (b) 0.5 wt % W-doped, (c) 1 wt % W-doped, and (d) 1.5 wt % W-doped deposited at 450 °C. (e) Cross-sectional view of 1 wt % W-doped SnO_2 thin film.

FESEM micrographs is consistent with variation of fwhm from XRD measurements.

The morphology and roughness of the pure and W-doped thin films is further investigated by the tapping-mode AFM. 3-D Atomic force micrographs of pure and W-doped SnO_2 films are shown in Figure 6a–d. The pure, 0.5 and 1.5 wt % W-doped films exhibit larger globules of particles of ∼50 nm size as compared to the 1 wt % W-doped films, which instead show smaller particles with ∼20 nm size. Further, it is also observed that in the case of pure, 0.5 and 1.5 wt % W-doped films the surface agglomerates are elongated whereas in 1 wt % W-doped SnO_2 film grains are mostly spherical in nature (see Figure 6). The topographical images reveal good quality of the films and surface roughness is found to increase with increase in W content. Root mean square (RMS) roughness values estimated for 0, 0.5, 1, and 1.5 wt % W-doped films using WSxM software, are 1.25, 1.36, 3.01, and 1.5 nm, respectively. The high roughness values are known to enhance gas sensitivity as film roughness is known to increase the porosity of the films.[31]

Gas sensing experiments were carried out by home-built sensing setup[28] in temperature range of 100–350 °C to find the optimum operating temperature. The gas sensor response is defined as

$$S_O = \frac{R_a - R_g}{R_g} \times 100 \text{ (for oxidizing gas)} \quad (2)$$

DOI: 10.1021/am507397z
ACS Appl. Mater. Interfaces 2015, 7, 3571–3580

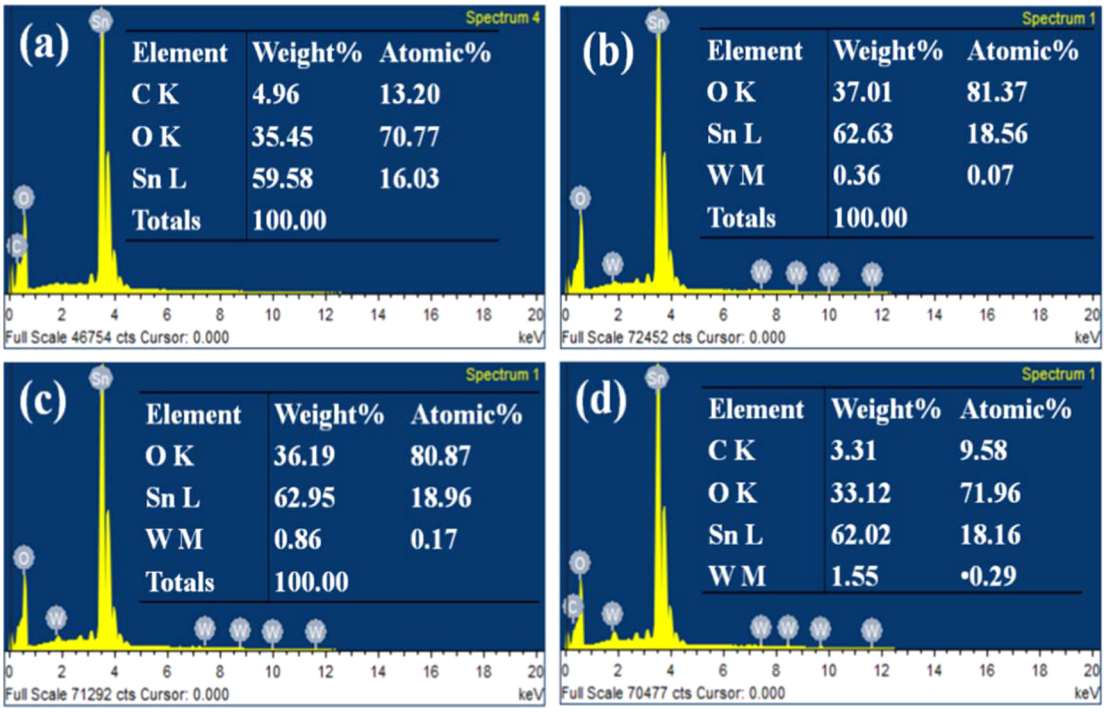

Figure 5. Shows EDS patterns of (a) pure SnO_2, (b) 0.5 wt % W-doped, (c) 1 wt % W-doped, and (d) 1.5 wt % W-doped deposited at 450 °C.

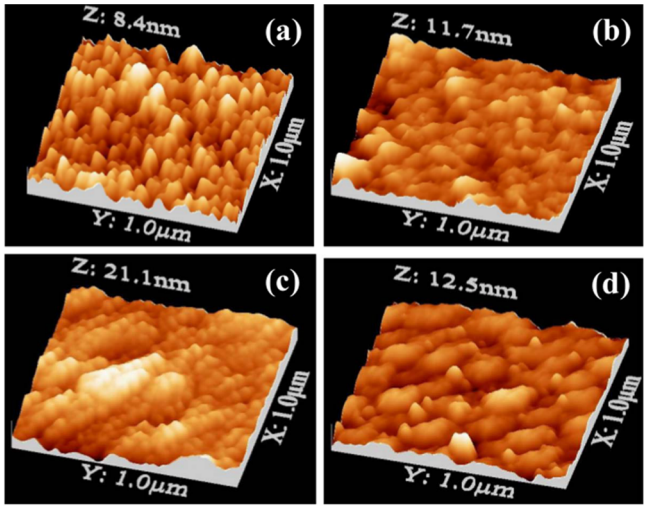

Figure 6. AFM topological micrographs in 3-D view of (a) pure SnO_2, (b) 0.5 wt % W-doped, (c) 1 wt % W-doped, and (d) 1.5 wt % W doped deposited at 450 °C.

$$S_R = \frac{R_g - R_a}{R_a} \times 100 \text{ (for reducing gas)} \quad (3)$$

where R_g is the electrical resistance in the presence of gas and R_a is the electrical resistance in clean synthetic air atmosphere only. Figure 7a displays the best sensing response shown by 1 wt % W-doped films for 400 ppm level of NO_2 gas at optimum operating temperature of 225 °C. It also shows faster response (recovery) times of the order of ~2 s (25 s). Figure 7b indicates that change in the resistance of sensor films is not only reproducible but proportional to the different ppm levels of NO_2. On the other hand 0.5 wt % W-doped sensors display very small sensitivity even at elevated temperatures of 275 °C and poor sensing response and recovery times of the order of ~5 s (150 s) as seen from Figure 7c. The sensor response measurements for W- doped sample shows improved response and recovery time as compared to reported values from the literature (see Table 1). Figure 8a displays sensor response variations, for different concentrations of NO_2, at optimum operating temperatures. Sensors responses increase almost linearly with NO_2 concentration up to 400 ppm. The sensor responses get saturated above 400 ppm of NO_2 exposure. It is evident from Figure 8 (a), 1 wt % W-doped sensor films show highest response of 132 for 400 ppm of NO_2. The sensor response of pure and W-doped sensors as a function of temperature for 400 ppm of NO_2 is shown in Figure 8(b). The maximum response has been observed at 225 °C in 1 wt % W-doped sensor, whereas in pure SnO_2 the poor sensor response increases almost linearly up to 325 °C. The maximum sensitivity, faster response and recovery times are observed for 1 wt % W-doped SnO_2 sensor films. Selectivity of the sensor films also was tested with 400 ppm of C_2H_5OH (ethanol), NH_3 (ammonia) and NO_2 gas. The sensor response values for all the above-mentioned gases are shown in Figure 9, which reveals that 1 wt % W-doped SnO_2 film is highly selective to NO_2 gas at its working temperature of 225 °C.

4. DISCUSSION

It has been demonstrated that, when exposed to NO_2 gas among all the sensors, the 1 wt % W-doped sensor films exhibit maximum sensitivity of (S_R = 132), faster response (~1−2 s), and least recovery time (~20−25 s) among all the films for 100 to 400 ppm levels of NO_2. The adsorption of NO_2 molecules occurs at the surfaces in two steps.[32] Initially, oxygen (O_2) molecules are adsorbed on the surface when the film is heated in the air, this leads to increase in resistance of the sensor material by creation of Schottkey barrier.[33] In second reaction, the oxidizing gases (like NO_2) injected into the reaction chamber reacts with the chemisorbed oxygen, (O^-)(ads) at the surface. The NO_2 molecules after interacting with the oxygen

DOI: 10.1021/am507397z
ACS Appl. Mater. Interfaces 2015, 7, 3571−3580

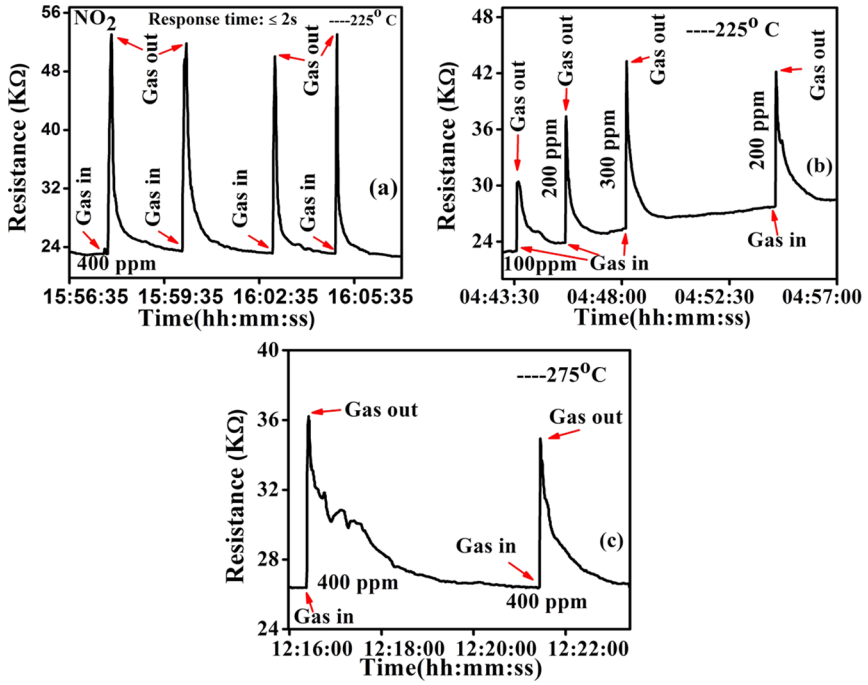

Figure 7. (a) Reproducibility of 1 wt % W-doped sensor response for 400 ppm of NO_2 at 225 °C. (b) Changes in sensing response exhibited for 100, 200, and 300 ppm of NO_2 by 1 wt % W-doped sensor at 225 °C, and (c) response of 0.5 wt % W-doped sensor for 400 ppm of NO_2 at 275 °C.

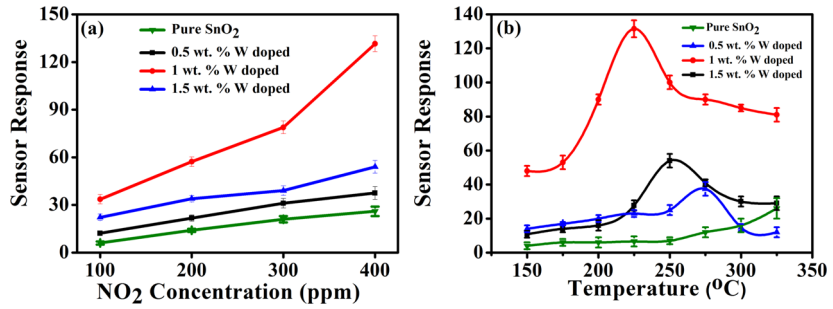

Figure 8. (a) Linearity of sensor response shown over concentration of 100−400 ppm of NO_2 for pure and W-doped SnO_2 and (b) sensor response as a function of operating temperature for pure and W-doped SnO_2, respectively, at 400 ppm of NO_2.

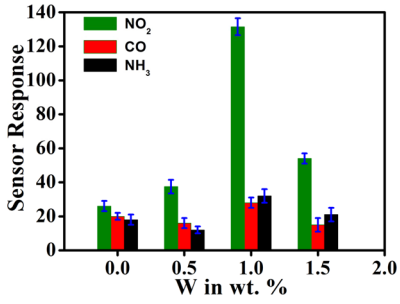

Figure 9. Sensor response of pure and W-doped SnO_2 as a function of W concentration at 400 ppm of each C_2H_5OH, NH_3, and NO_2 gas.

species adsorbed on the sensors surface, reduce the electron concentration and therefore, an increase in the electrical resistance occurs. The chemisorbed oxygen ions react with NO_2 gas accordingly the following reaction path.[15]

$$SnO_2 + e^- + \frac{1}{2}O_2 \leftrightarrow SnO_2(O^-)\ (ads) \quad (4)$$

$$SnO_2 + (O^-)\ (ads) + NO_2 \rightarrow SnO_2 + NO^{2-}\ (ads) \quad (5)$$

The CSP synthesized pure SnO_2 nanocrystalline films were found to having texture along (110) plane when deposited at temperature, T = 425 °C.[14] The first principal calculations have shown that (110) reduced plane has higher surface energy of as compared to stoichiometric (110) plane.[34] The stability of reduced (110) surfaces in[10] real sensors (which are essentially nonstoichiometric) must then be probably ensured by increasing higher atomic planar density, reflected in higher texture coefficient of (110). Computer image simulations of CSP deposited films, at T = 425 °C and having crystallite size of 30−60 nm, revealed growth of SnO_2 crystals along [110] direction which has other crystalline surfaces like (200), (111), (101), and (011) planes.[14] In light of this it is possible that W-doping in SnO_2 nanostructured films synthesized using CSP can lead to atomic displacements within the unit cell such that planar atomic density of (110) reduces at the cost of increase in (200) plane as reflected in the texture analysis presented here. In CSP deposited films migration of Sn and O atoms from (110) plane to (200) plane is feasible as (110) orientation has a high atomic density and (200) orientation has a low atomic planar density[35,36] in tetragonal rutile phase of SnO_2 in the first place see in Figure 2a and b and more importantly (110)

DOI: 10.1021/am507397z
ACS Appl. Mater. Interfaces 2015, 7, 3571−3580

surfaces are enclosed by (200) planes.[37] This fact is further highlighted by plotting integrated intensity ratio's of I_{200}/I_{110} planes against W-doping in wt % as shown in Figure 2d. It is observed that I_{200}/I_{110} for 1 wt % W-doped films (0.201) is almost twice than that of remaining films. This large increase in I_{200}/I_{110} suggest that atomic planar density of (200) planes increases at the cost of (110) planes which results vacancies on (110) plane. Thus, reduction of texture coefficient along (110), in particular 1 wt % W-doped films is symptomatic of reduced (110) surfaces.[34] The highest sensitivity for 1 wt % W-doped films, as seen from Table 2, in the present work, is attributed to large reduction in texture coefficient occurred along densely packed (110) plane with concomitant increase in (200) plane. Reduced (110) surfaces, in 1 wt % W-doped SnO_2, have higher surface energy because of creation of more vacancies which then can act as a better sight for adsorption of NO_2 molecules due to many unsaturated bonds available on the (110) plane that in turn is attributed to higher sensor response. In recent report[38] on fluorine doped SnO_2, increase in preferred orientation along (200) plane with concurrent decrease along (110) is shown to be associated with increase in high carrier concentration and mobility, which in turn improves the conductivity of SnO_2 films. The better sensor response observed in 1 wt % W-doped films thus may be attributed to increase in texture coefficient of (200) plane observed in the present study. In other study, fluorine doping in SnO_2 films is reported to increase (decrease) the electrical resistivity with increase (decrease) in texture along least dense (200) plane.[39] Non-stoichiometric NiO films reveal (111)-preferred orientation on the other hand stoichiometric NiO films exhibit (200) texture. It is to be noted that (111) [(200)] plane has least (more) planar density in NiO system. Because of these effects sheet resistance and resistivity decrease for (111) oriented NiO films.[40] The present results in 1 wt % W-doped samples where base resistance is found decreased is attributed to increase in texture coefficient in (200) plane. Decrease in crystallite size, d, determined by XRD measurements is comparable to Debye length, L (where $2L \approx d$ nm) in case of 1 wt % W-doped film is attributed to produce marked changes in the film surfaces[21,41] that enhances the sensitivity. The average crystallite size estimated from XRD analysis is ∼6 nm also suggest that grain boundary area or interfaces reflected in porous microstructure in FESEM is quite larger as compared with other films. Because estimated average grain size from FESEM studies (∼10 nm) is comparable with average crystallite size determined by XRD measurements. Another important microstructural feature observed in FESEM micrographs of 1 wt % W-doped film is clustering of small nanosized grains in contrast to the other films where homogeneous uniform grain size distribution is observed (see Figure 4). The close scrutiny of 1 wt % W-doped film microstructure reveals that nanocrystalline grains are agglomerated. The agglomeration of small crystallizes into large masses on the sensor surfaces is known to improve the gas sensitivity.[37] From AFM studies it is clear that film roughness is higher in case of 1 wt % W-doped films. Increase in sensing response because of higher RMS roughness values is already reported in literature.[42,43] The increase in texture coefficient observed in low atomic density plane, in the present study, may explain the mechanism behind these observations. As increase in texture coefficient along (200) results in grain boundary mismatch which further improves the porosity in thin film microstructures. The increased porosity leads to agglomeration which is reflected in increased roughness values observed in 1 wt % W-doped SnO_2 films. The increased porous network is also responsible for permeation of incoming gas molecules which enhance adsorption and desorption mechanisms responsible for higher sensitivity and enhanced recovery and response times observed in 1 wt % W-doped films.[37] It is important to notice at this stage that increased texture along low density (200) Miller plane may thus, result in large values of RMS roughness (3.1) observed for 1 wt % doped films. The optical band gap energy of 3.82 eV estimated for 1 wt % W-doped thin films is lowest among the other doped films. Optical band gap depends on changes in crystal bonding as well as on lattice constants.[34] However, in nanosrystalline thin films of metal oxide semiconductors like SnO_2, expansion or contraction of space charge layer in the presence of different gases, conduction can change drastically.[44,45] Density of surface states induced by chemisorbed oxygen species increase with lower crystallite size which can reduce band gap due to pinning of Fermi surfaces.[46] Detailed ultra photoemission spectroscopy studies revealed that oxygen deficient (110) surfaces of SnO_2 show a significant density of surface states in the band gap up to Fermi level, but oxidized or stoichiometric surfaces exhibit no significant density of band gap states.[47] Thus, W-doping in SnO_2 lattice can alter the band structure[21] such that band gap decreases with initial increase in W doping concentration up to 1 wt %. Decrease in band gap is also associated with increase in oxygen vacancies within the SnO_2 lattice.[48] Largest sensing response observed in 1 wt % W-doped is related to increased oxygen vacancies in SnO_2 lattice that provides an active site for adsorption of NO_2 gas molecules.[42] Realizing the fact that reduction in integrated intensity ratio of (I_{200}/I_{110}) and texture coefficient of (110) plane in 1 wt % W-doped films may result in creation of oxygen deficient surfaces. These reduced (110) surfaces are known to create additional energy levels near valence band because of formation of unsaturated bonds.[49] The reduced band gap energy is thus intimately related to reduction of texture coefficient in 1 wt % W-doped films. It is evident that the changes in atomic planar density in W-doped thin films can modify morphological, structural, and optical properties such that sensitivity of NO_2 is enhanced along with faster recovery times.

5. CONCLUSIONS

Thus, in conclusion, we have synthesized pure and W-doped tin oxide thin films by simple and inexpensive CSP technique for the first time. W-doping improves the sensor response and selectivity toward NO_2 gas. The texture analysis indicates that pure SnO_2 films are textured along (110) plane. However, with 1 wt % W-doping, the texture coefficient of (200) plane increases remarkably at the expense of (110) plane. Reduction in texture coefficient of (110) plane can create many unsaturated bonds across the plane which then act as preferable sight for adsorption of NO_2 molecules reflected in higher sensing response. A high sensor response of 132 was observed in the case of 1 wt % W-doped SnO_2 thin films to 400 ppm of NO_2 gas at a low operating temperature of 225 °C. The increase in texture coefficient of low atomic planar density (200) plane is found to affect clustering of nanosized grains, increase in RMS roughness and decrease in band gap energy in 1 wt % W-doped SnO_2 films.

DOI: 10.1021/am507397z
ACS Appl. Mater. Interfaces 2015, 7, 3571−3580

■ ASSOCIATED CONTENT

Supporting Information

Particle size distribution of W-doped thin films. This material is available free of charge via the Internet at http://pubs.acs.org.

■ AUTHOR INFORMATION

Corresponding Author

*Tel.: +91-20-24304311. E-mail: ashutosh@diat.ac.in, ashutoshabhyankar@gmail.com.

Notes

The authors declare no competing financial interest.

■ ACKNOWLEDGMENTS

All the authors acknowledge Vice Chancellor, Defence Institute of Advance Technology (DIAT) for his constant support and encouragement. Dr. Suwarna Datar and Promod Bankar are acknowledged for AFM measurements. A.C.A. and M.K. would like to acknowledge financial assistance from ERIP/ER/1003883/M/01/908/2012/D(R&D)/1416 project.

■ REFERENCES

(1) Comini, E.; Faglia, G.; Sberveglieri, G. Stable and Highly Sensitive Gas Sensors Based on Semiconducting Oxide Nanobelts. *Appl. Phys. Lett.* **2002**, *81*, 1869−1871.

(2) Korotcenkov, G. The Role of Morphology and Crystallographic Structure of Metal Oxides in Response of Conductometric-Type Gas Sensors. *Mater. Sci. Eng., R* **2008**, *61*, 1−39.

(3) Katoch, A.; Sun, G. J.; Choi, S. W.; Hishita, S.; Kulish, V. V.; Wu, P.; Kim, S. S. Acceptor-Compensated Charge Transport and Surface Chemical Reactions in Au-Implanted SnO_2 Nanowires. *Sci. Rep.* **2014**, *4*, No. 4622, DOI: 10.1038/srep04622.

(4) Li, Z.; Zhao, Q.; Fan, W.; Zhan, J. Porous SnO_2 Nanospheres as Sensitive Gas Sensors for Volatile Organic Compounds Detection. *Nanoscale* **2011**, *3*, 1646−1652.

(5) Chen, S.; Wang, M.; Ye, J.; Cai, J.; Ma, Y.; Zhou, H.; Qi, L. Kinetics-Controlled Growth of Aligned Mesocrystalline SnO_2 Nanorod Arrays for Lithium-ion Batteries with Superior Rate Performance. *Nano Res.* **2013**, *6* (4), 243−252.

(6) Shi, L.; Xu, Y.; Li, Q. Controlled Fabrication of SnO_2 Arrays of Well-Aligned Nanotubes and Nanowires. *Nanoscale* **2010**, *2*, 2104−2108.

(7) Devan, R. S.; Patil, R. A.; Lin, J. H.; Ma, Y. R. One-Dimensional Metal-Oxide Nanostructures: Recent Developments in Synthesis, Characterization, and Applications. *Adv. Funct. Mater.* **2012**, *22*, 3326−3370.

(8) Hassan, M. A. M.; Hateef, A. A.; Majeed, A. M. A.; Al-Jabiry, A. J. M.; Jameel, S.; Hussian, H. A. R. A. Amperometric Biosensor of SnO_2 Thin Film Modified by Pd, In and Ag Nanostructure Synthesized by CSP Method. *Appl. Nanosci.* **2014**, *4*, 927−934.

(9) Zeng, J.; Hu, M.; Wang, W.; Chen, H.; Qin, Y. NO_2-Sensing Properties of Porous WO_3 Gas Sensor Based on Anodized Sputtered Tungsten Thin Film. *Sens. Actuators, B* **2012**, *161*, 447−452.

(10) Batzill, M.; Diebold, U. The Surface and Materials Science of Tin Oxide. *Prog. Surf. Sci.* **2005**, *79*, 47−154.

(11) Kaneti, Y. V.; Zhang, Z.; Yue, J.; Zakaria, Q. M. D.; Chen, C.; Jiang, X.; Yu, A. Crystal Plane-Dependent Gas-Sensing Properties of Zinc Oxide Nanostructures: Experimental and Theoretical Studies. *Phys. Chem. Chem. Phys.* **2014**, *16*, 11471−11480.

(12) Yue, J.; Jiang, X.; Yu, A. Adsorption of the OH Group on SnO_2(110) Oxygen Bridges: A Molecular Dynamics and Density Functional Theory Study. *J. Phys. Chem. C* **2013**, *117*, 9962−9969.

(13) Gurlo, A. Nanosensors: Towards Morphological Control of Gas Sensing Activity. SnO_2, In_2O_3, ZnO, and WO_3 Case Studies. *Nanoscale* **2011**, *3*, 154−165.

(14) Korotcenkov, G.; Cornet, A.; Rossinyol, E.; Arbiol, J.; Brinzari, V.; Blinov, Y. Faceting Characterization of Tin Dioxide Nanocrystals Deposited by Spray Pyrolysis from Stannic Chloride Water Solution. *Thin Solid Films* **2005**, *471*, 310−319.

(15) Wetchakun, K.; Samerjai, T.; Tamaekong, N.; Liewhiran, C.; Siriwong, C.; Kruefu, V.; Wisitsoraat, A.; Tuantranont, A.; Phanichphant, S. Semiconducting Metal Oxides as Sensors for Environmentally Hazardous Gases. *Sens. Actuators, B* **2011**, *160*, 580−591.

(16) Zampetti, E.; Macagnano, A.; Pantalei, S.; Bearzotti, A. PEDOT:PSS-Coated Titania Nanofibers for NO_2 Detection: Study of Humidity Effects. *Sens. Actuators, B* **2013**, *179*, 69−73.

(17) Lee, D. S.; Lim, J. W.; Lee, S. M.; Huh, J. S.; Lee, D. D. Fabrication and Characterization of Micro-Gas Sensor for Nitrogen Oxides Gas Detection. *Sens. Actuators, B* **2000**, *64*, 31−36.

(18) Kim, K. W.; Cho, P. S.; Kim, S. J.; Lee, J. H.; Kang, C. Y.; Kim, J. S.; Yoon, S. J. The Selective Detection of C_2H_5OH using SnO_2−ZnO Thin Film Gas Sensors Prepared by Combinatorial Solution Deposition. *Sens. Actuators, B* **2007**, *123*, 318−324.

(19) Sharma, A.; Tomar, M.; Gupta, V. SnO_2 Thin Film Sensor with Enhanced Response for NO_2 Gas at Lower Temperatures. *Sens. Actuators, B* **2011**, *156*, 743−752.

(20) Sharma, A.; Tomar, M.; Gupta, V. WO_3 Nanoclusters−Sno_2 Film Gas Sensor Heterostructure with Enhanced Response for NO_2. *Sens. Actuators, B* **2013**, *176*, 675−684.

(21) Huang, Y.; Zhang, Q.; Li, G. Transparent Conductive Tungsten-Doped Tin Oxide Polycrystalline Films Prepared on Quartz Substrates. *Semicond. Sci. Technol.* **2009**, *24*, 015003.

(22) Dominguez, J. E.; Fu, L.; Pan, X. Q. Effect of Crystal Defects on the Electrical Properties in Epitaxial Tin Dioxide Thin Films. *Appl. Phys. Lett.* **2002**, *81*, 5168−5170.

(23) Kaur, J.; Vankar, V. D.; Bhatnagar, M. C. Effect of MoO_3 Addition on the NO_2 Sensing Properties of SnO_2 Thin Films. *Sens. Actuators, B* **2008**, *133*, 650−655.

(24) Kaur, J.; Roy, S. C.; Bhatnagar, M. C. Highly Sensitive SnO_2 Thin Film NO_2 Gas Sensor Operating at Low Temperature. *Sens. Actuators, B* **2007**, *123*, 1090−1095.

(25) An, S.; Park, S.; Ko, H.; Lee, C. Fabrication of WO_3 Nanotube Sensors and Their Gas Sensing Properties. *Ceram. Int.* **2014**, *40*, 1423−1429.

(26) Yan, W.; Hu, M.; Zeng, P.; Ma, S.; Li, M. Room Temperature NO_2-Sensing Properties of WO_3 Nanoparticles/Porous Silicon. *Appl. Surf. Sci.* **2014**, *292*, 551−555.

(27) Batzill, M.; Diebold, U. Surface Studies of Gas Sensing Metal Oxides. *Phys. .Chem. Chem. Phys.* **2007**, *9*, 2307−2318.

(28) Kumar, M.; Kumar, A.; Abhyankar, A. C. SnO_2 Based Sensors with Improved Sensitivity and Response-Recovery Time. *Ceram. Int.* **2014**, *40*, 8411−8418.

(29) Harris, G. B. X. Quantitative Measurement of Preferred Orientation in Rolled Uranium Bars. *Philos. Mag.* **1952**, *43*, 113−123.

(30) Cullity, D. B. *Elements of X-ray Diffraction* , 2nd ed.; Addision-Wesley: Reading, MA, 1978.

(31) Deshpande, N. G.; Gudage, Y. G.; Sharma, Y. G.; Vyas, J. C.; Kim, J. B.; Lee, Y. P. Studies on Tin Oxide-Intercalated Polyaniline Nanocomposite for Ammonia Gas Sensing Applications. *Sens. Actuators, B* **2009**, *138*, 76−84.

(32) Zhang, C.; Debliquy, M.; Boudiba, A.; Liao, H.; Coddet, C. Sensing Properties of Atmospheric Plasma-Sprayed WO_3 Coating for Sub-ppm NO_2 Detection. *Sens. Actuators, B* **2010**, *144*, 280−288.

(33) McAleer, J. F.; Moseley, P. T.; Norris, J. O. W.; Williams, D. E.; Tofield, B. C. Tin Dioxide Gas Sensors. Part 2—The Role of Surface Additives. *J. Chem. Soc., Faraday Trans. 1* **1988**, *84*, 441−457.

(34) Bergermayer, W.; Tanaka, I. Reduced SnO_2 Surfaces by First-Principles Calculations. *Appl. Phys. Lett.* **2004**, *84*, 909−911.

(35) Fantini, M.; Torriani, I. L.; Constantino, C. Influence of the Substrate on the Crystalline Properties of Sprayed Tin Dioxide Thin Films. *J. Cryst. Growth* **1986**, *74*, 439−442.

(36) Korotkov, R. Y.; Ricou, P.; Farran, A. J. E. Preferred Orientations in Polycrystalline SnO_2 Films Grown by Atmospheric Pressure Chemical Vapor Deposition. *Thin Solid Films* **2006**, *502*, 79−87.

DOI: 10.1021/am507397z
ACS Appl. Mater. Interfaces 2015, 7, 3571−3580

(37) Korotcenkov, G. Gas Response Control Through Structural and Chemical Modification of Metal Oxide Films: State of the Art and Approaches. *Sens. Actuators, B* **2005**, *107*, 209−232.
(38) Wang, J. T.; Shi, X. L.; Liu, W. W.; Zhong, X. H.; Wang, J. N.; Pyrah, L.; Sanderson, K. D.; Ramsey, P. M.; Hirata, M.; Tsuri, K. Influence of Preferred Orientation on the Electrical Conductivity of Fluorine-Doped Tin Oxide Films. *Sci. Rep.* **2014**, *4*, No. 3679, DOI: 10.1038/srep03679.
(39) Moholkar, A. V.; Pawar, S. M.; Rajpure, K. Y.; Bhosale, C. H.; Kim, J. H. Effect of Fluorine Doping on Highly Transparent Conductive Spray Deposited Nanocrystalline Tin Oxide Thin Films. *Appl. Surf. Sci.* **2009**, *255*, 9358−9364.
(40) Chen, H. L.; Yang, Y. S. Effect of Crystallographic Orientations on Electrical Properties of Sputter-Deposited Nickel Oxide Thin Films. *Thin Solid Films* **2008**, *516*, 5590−5596.
(41) Golovanov, V.; Korotcenkov, G.; Brinzari, V.; Cornet, A.; Morante, J.; Arbiol, J.; Russinyol, E. CO−Water Interaction with SnO_2 Gas Sensors: Role of Orientation Effects. *Transducers Eurosens. XVI, Int. Conf. Solid-State Sens., Actuators Microsyst., 16th* **2002**, 926−929.
(42) Kaur, J.; Kumar, R.; Bhatnagar, M. C. Effect of Indium-Doped SnO_2 Nanoparticles on NO_2 Gas Sensing Properties. *Sens. Actuators, B* **2007**, *126*, 478−484.
(43) Rani, S.; Roy, S. C.; Bhatnagar, M. C. Effect of Fe doping on Gas Sensing Properties of Nanocrystalline SnO_2 Thin Films. *Sens. Actuators, B* **2007**, *122*, 204−210.
(44) Puzder, A.; Williamson, A. J.; Reboredo, F. A.; Galli, G. Structural Stability and Optical Properties of Nanomaterials with Reconstructed Surfaces. *Phys. Rev. Lett.* **2003**, *91*, No. 157405.
(45) Maffeis, T. G. G.; Owen, G. T.; Penny, M. W.; Starke, T. K. H.; Clark, S. A.; Ferkel, H.; Wilks, S. P. Nano-Crystalline SnO_2 Gas Sensor Response to O_2 and CH_4 at Elevated Temperature Investigated by XPS. *Surf. Sci.* **2002**, *520*, 29−34.
(46) Maffeis, T. G. G.; Owen, G. T.; Malagu, C.; Martinelli, G.; Kennedy, M. K.; Kruis, F. E.; Wilks, S. P. Direct Evidence of the Dependence of Surface State Density on the Size of SnO_2 Nanoparticles Observed by Scanning Tunnelling Spectroscopy. *Surf. Sci.* **2004**, *550*, 21−25.
(47) Cox, D. F.; Fryberger, T. B.; Semancik, S. Oxygen Vacancies and Defect Electronic States on the SnO_2 (110)-1 × 1 Surface. *Phys. Rev. B* **1988**, *38*, 2072−2083.
(48) Drake, C.; Seal, S. Band Gap Energy Modifications Observed in Trivalent In Substituted Nanocrystalline SnO_2. *Appl. Phys. Lett.* **2007**, *90*, No. 233117.
(49) Hartman, P. *Crystal Growth: An Introduction*; North-Holland: Amsterdam, 1973; pp 367−402.

DOI: 10.1021/am507397z
ACS Appl. Mater. Interfaces 2015, 7, 3571−3580